Research Article

# Synergistic Removal of 4-Chloroaniline from Contaminated Water via Biochar-enhanced Microbial Degradation and Adsorption Using Carbonized Wood Waste

Taksaporn Boonta, Supitchaya Jenjaiwit, Panitan Jutaporn, Thunyalux Ratpukdi and Sumana Siripattanakul-Ratpukdi*
Department of Environmental Engineering, Faculty of Engineering and Research Center for Environmental and Hazardous Substance Management, Khon Kaen University, Khon Kaen, Thailand

* Corresponding author. E-mail: sumana.r@kku.ac.th DOI: 10.14416/j.asep.2026.02.008
Received: 5 October 2025; Revised: 14 November 2025; Accepted: 22 December 2025; Published online: 17 February 2026


**Abstract**
4-chloroaniline (4-CA) is a widely used aromatic amine, resulting in contamination in aquatic environments. Due to its high toxicity and persistence, 4-CA has been designated as a priority pollutant. This study aims to investigate 4-CA removal using an integrated system of biochar (carbonized wood waste) and *Bacillus subtilis* GRSW2-B1 (GRSW2-B1). The study consists of three parts: 1) evaluation of 4-CA removal by biochar, GRSW2-B1, and biochar and GRSW2-B1 combination, 2) investigation of 4-CA degradation kinetics, and 3) examination of the role of biochar in 4-CA removal. The result showed that biochar provided good 4-CA adsorption, following the Langmuir model, with a maximum capacity of 4.9 mg/g. The combined system of biochar and microbial cells (designated as BC-G1) achieved a removal efficiency of up to 73%, while microorganism alone (G1) yielded a value of 45%. For the 4-CA degradation kinetics, both G1 and BC-G1 systems followed the Andrews model, with an inhibition concentration of 65 mg/L. Field-emission scanning electron microscopy (FE-SEM), Fourier transform infrared (FTIR) spectroscopy, and fluorescence excitation-emission matrix (EEM) spectroscopy revealed that biochar enhanced 4-CA removal via: 1) adsorption on the biochar surface and stimulation of extracellular polymeric substance (EPS) production, and 2) enhancing biodegradation by facilitating redox-related electron transfer. The EPS-related functional groups, aromatic proteins, and fulvic and humic acid-like compounds showed increased levels in BC-G1, which is associated with electron shuttling and mediation processes. Overall, the integration of biochar and microbial cells significantly improved 4-CA removal, highlighting a promising, sustainable approach for the remediation of emerging toxic contaminants.

**Keywords**: Aniline, Biodegradation, Carbonized waste, Electron transfer, Extracellular polymeric substance

## 1 Introduction

Among chlorinated organic compounds, 4–chloroaniline (4–CA) is a widely used aromatic amine in various industrial, agricultural, and pharmaceutical products, such as dyes, pesticides, and antiseptics [1]. Its extensive use has led to widespread 4–CA contamination in wastewater and natural water worldwide. For example, 4–CA levels of up to 2.4 µg/L have been reported in the Yangtze River area, China, posing a high ecological risk [2]. 4–CA is highly toxic, recalcitrant, and bioaccumulative and has been classified as a priority pollutant by the United States Environmental Protection Agency [3]. This necessitates the development of effective water treatment technologies for the removal of 4–CA contamination.

To date, several physicochemical methods have been investigated for removing xenobiotics, including 4-CA. Among these, adsorption is a widely applied and reliable technique due to its simplicity, high efficiency, cost–effectiveness, and rapid removal capabilities. Further, it has been successfully employed for the removal of aromatic amines [4]. Recently, biochar–a carbon–rich material produced through the pyrolysis of agricultural and agro–

industrial waste–has gained attention as an adsorbent for environmental treatment, especially in the removal of emerging toxic contaminants. Biochar possesses a high surface area and is rich in surface functional groups, enabling the effective adsorption of both contaminants and microorganisms. The application of biochar has recently been expanded to increase redox–related electron transfer by serving as an electron shuttle, which enhances biodegradation processes, such as anaerobic digestion and emerging contaminant removal [5], [6]. In terms of 4–CA removal, biochar facilitates 4–CA adsorption and degradation [7], [8]. The previous work reported that biochar successfully adsorbed 4–CA. However, to prepare biochar from raw feedstock, energy is required, while air emission is concerned. Recently, industrial wood pyrolysis in bio–oil or wood vinegar production has generated a substantial amount (approximately 30% of feedstock) of carbonized wood waste [9]. Carbonized waste with a large surface area and diverse functional groups is promising for direct application as biochar, contributing to the sustainable utilization of resources and enhanced carbon sequestration [10].

For long–term application, the adsorption process alone may be limited because adsorbents require frequent replacement and maintenance to sustain performance, therefore, biological treatment processes may be an economical and sustainable alternative. Microbial degradation is an extensively applied technique for toxic contaminants, including chloroanilines. The technique is environmentally friendly, cost–effective, and has operational simplicity. Furthermore, biodegradation can contribute to contaminant detoxification. Previously, effective 4–CA degrading bacterial strains, such as *Acinetobacter baylyi* GFJ2 [11] and *Pseudomonas* sp. CA–1 [12] has been studied. However, in real–world scenarios, industrial and agricultural wastewater often contains various toxic compounds, which may influence the survival of microorganisms and the activity of specific degrading microorganisms. Therefore, the ability of previously isolated strains to degrade co–existing contaminants has been tested to enhance their potential for practical application. *Bacillus subtilis* GRSW2–B1 (GRSW2–B1), a butanol–tolerant bacterium, has demonstrated resistance to various organic solvents and alcohols [13]. Our preliminary study has also shown that GRSW2–B1 can effectively degrade various chlorinated pesticides, including 4–CA. We found that GRSW2–B1 achieved more than 30% removal of 4–CA.

In practice, direct microbial augmentation may cause cell mitigation from contaminated environments. Therefore, integrated microorganism and biochar augmentation has been widely adopted as a strategy for the removal of emerging contaminants, as biochar not only adsorbs contaminants but also serves as a microbial support [14], protecting microbial cells from direct exposure to toxic contaminants. Furthermore, studies have increasingly recognized the role of biochar in facilitating extracellular electron transfer during biological treatment processes [6], [14], [15].

Limited studies have applied the concept of integrated biochar–microbial cell augmentation for the treatment of chlorinated hydrocarbons [16]. To date, no study has focused on the integrated biochar–microbial cell application for the remediation of chlorinated aniline contamination. This research gap has been addressed herein by combining biochar, derived from carbonized waste from wood vinegar production, and GRSW2–B1, a bacterial strain capable of degrading 4–CA. This work aimed to investigate 4–CA removal using biochar, free GRSW2–B1 cells, and their combination. Kinetic analyses were conducted to assess 4–CA degradation by GRSW2–B1 cells and their combination with biochar for various initial concentrations. Some previous studies showed that biochar can stimulate extracellular polymeric substances (EPSs) and enhance direct interspecies electron transfer (DIET) in microbial communities [17]. To the best of our knowledge, this is the first study to explore the role of biochar in relation to EPSs secreted by microbial cells and DIET induced by biochar during 4–CA removal. Fourier transform infrared (FTIR) spectroscopy and fluorescence excitation–emission matrix (EEM) spectroscopy were used as characterization techniques. The findings provide insights into treatment performance and parameters for the design and optimization of systems targeting 4–CA and other emerging contaminants. Furthermore, this research aligns with Sustainable Development Goal 6, which promotes integrated water resource management and the sustainable, environmentally responsible use of water resources.

## 2 Materials and Methods

### 2.1 *Chemicals*

Analytical–grade 4–CA (98% purity) and its degradation intermediates, including 4–chlorocatechol

(4–CC) (97% purity), aniline (AN) (99% purity), and catechol (CT) (99% purity), were purchased from Sigma–Aldrich (MO, USA). All other laboratory–grade chemicals used for the bacterial culture media, synthetic contaminated wastewater preparation, and analytical procedures were obtained from local distributors.

### 2.2 *Biochar preparation*

The crushed carbonized waste was acquired from an industrial wood vinegar production plant in Ubon Ratchathani, Thailand, with the wood vinegar production process lasting 4 weeks. The bamboo trunks were pyrolyzed at 800 °C under oxygen–limited conditions for 14 days, followed by gradual cooling over another 14 days. The industrial carbonized waste was crushed before commercialization. The crushed biochar was prepared following the method described earlier by Sonsuphab *et. al.,* [18]. The biochar (200 g) was then heated at 800 °C under pyrolytic conditions and sieved using U.S. standard sieve numbers 5 and 10 to obtain 2–4–mm biochar. The biochar was subsequently rinsed with reverse osmosis water, dried at 103 °C overnight, and autoclaved twice before use.

### 2.3 *Bacterium and cultivation*

The augmented bacterium, *Bacillus subtilis* GRSW2–B1 (GenBank accession number HQ912916), has been previously reported by Kataoka *et. al.,* [13]. The GRSW2–B1 strain was initially cultivated in Luria–Bertani (LB) medium supplemented with 4–CA (designated as LB–4CA). The bacterial cultivation was modified from the method described earlier by Sonsuphab *et. al.,* [18]. The LB medium was prepared by dissolving 10 g of tryptone, 10 g of NaCl, and 5 g of yeast extract in 1 L of reverse osmosis water, and LB–4CA was prepared by supplementing the LB medium with 4–CA at a final concentration of 10 mg/L. Two loops of GRSW2–B1 were transferred from an LB-4CA agar plate into 10 mL of the LB–4CA liquid medium and incubated at room temperature with shaking at 150 rpm for 14 h. Following incubation, the culture was centrifuged at 6,000 rpm for 10 min. The concentrated cells were inoculated in 10 mL of fresh LB–4CA and incubated under the same conditions for an additional 14 h. The inoculated cells were then applied in the experimental investigations.

### 2.4 *4–chloroaniline removal*

The removal of 4–CA using the biochar, free GRSW2–B1 cells, and their combination (designated as BC, G1, and BC–G1, respectively) was investigated, and all experiments were conducted in triplicate. Each system contained 50 mL of 4–CA solution (or synthetic wastewater) and was prepared as follows: BC contained 0.5 g of biochar, G1 contained GRSW2–B1 at $10^7$ CFU/mL, and BC–G1 contained 0.5 g of biochar together with GRSW2–B1 at $10^7$ CFU/mL. The components were prepared separately and subsequently augmented into the 4–CA solution prior to the experiment.

The adsorption kinetics and isotherms of a 4–CA solution using BC were examined. Biochar (0.5 g) was added to a 10–mg/L 4–CA solution (50 mL) and shaken at 150 rpm for 48 h; water samples (0.5 mL) were taken at intervals to measure the remaining 4–CA concentration. The adsorption kinetics (pseudo–first–order and pseudo–second–order models) and isotherms (Langmuir and Freundlich models) and adsorption were analyzed due to their common application in biochar–based adsorption systems [7], [8], [10]. The isotherm and kinetic parameters were derived from the experimental data obtained in this study and validated using the coefficient of determination ($R^2$). The $R^2$ value was calculated within the scope of this study by fitting the experimental data to the corresponding kinetic and isotherm models using the least-squares regression method.

The 4–CA adsorption kinetics were assessed using pseudo–first–order and pseudo–second–order models (Table 1). In the isotherm study, 0.5 g of biochar was added to a 4–CA solution with initial concentrations ranging from 0.5 to 100 mg/L, and the mixtures were shaken at 150 rpm to achieve equilibrium (36 h). The concentration of 4–CA at the equilibrium time was fitted to the Langmuir and the Freundlich models (Table 1) to describe the adsorption behavior of 4–CA onto the biochar. The 4–CA remaining concentrations compared to the initial concentrations ($C/C_0$), representing 4–CA removal efficiencies, were shown in Figure 1

The removal of 4–CA by BC, G1, and BC–G1 was evaluated in LB–4CA medium (serving as a representative model of contaminated wastewater), with initial 4–CA concentrations ranging from 10 to 500 mg/L. In each setup, biochar (0.5 g) and/or GRSW2–B1 ($10^7$ CFU/mL) were added to the LB–

4CA medium (50 mL) and incubated with shaking at 150 rpm for 72 h. It is noted that the BC–G1 system contained the mixture of microbial cells and biochar throughout the experiment until sampling. Aliquots of the water samples (0.5 mL) were taken in intervals to measure the concentrations of 4–CA and its intermediate products. Selected biochar samples were characterized in terms of surface functional groups and morphological changes, while the water samples were analyzed for organic carbon compositions related to microbial secretion and EET.

**Table 1**: 4–CA adsorption kinetic and isotherm equations and parameters for the carbonized waste–derived biochar.

| | |
|---|---|
| **Adsorption kinetics** | |
| ***Pseudo-first-order reaction*** | |
| $\ln(Q_e - Q_t) = \ln Q_e - k_1 t$ | |
| $Q_t$ = Adsorption capacities at time (mg/g)<br>$Q_e$ = Adsorption capacities at equilibrium (mg/g)<br>$k_1$ = The pseudo-first-order reaction rate (1/min) | $Q_e$ = 47.078<br>$k_1$ = 0.0604<br>$R^2$ = 0.9882 |
| ***Pseudo-second-order reaction*** | |
| $\frac{t}{Q_t} = \frac{1}{k_2 Q_e^2} + \frac{t}{Q_e}$ | |
| $Q_t$ = Adsorption capacities at time (mg/g)<br>$Q_e$=Adsorption capacities at equilibrium (mg/g)<br>$k_2$ = The pseudo-second-order reaction rate (g/mg-min) | $Q_e$ = 0.0302<br>$k_2$ = 7.1126<br>$R^2$ = 0.9970 |
| **Adsorption isotherm** | |
| ***Langmuir model*** | |
| $\frac{1}{Q_e} = \frac{1}{k_L Q_m C_e} + \frac{1}{Q_m}$ | |
| $Q_e$ = Adsorption capacity at equilibrium (mg/g)<br>$Q_m$ = Maximum adsorption capacity (mg/g)<br>$C_e$ = Concentration at equilibrium (mg/L).<br>$k_L$ = Langmuir adsorption constant (L/mg) | $Q_m$= 4.9456<br>$K_L$= 1.3906<br>$R^2$ = 0.9713 |
| ***Freundlich model*** | |
| $\log Q_e = \log k_f + \frac{1}{n} \log C_e$ | |
| $Q_e$ = Adsorption capacity at equilibrium (mg/g)<br>$C_e$ = Concentration at equilibrium (mg/L).<br>$k_f$= Freundlich adsorption constant (mg/g)<br>n = adsorption intensity | n = 4.3103<br>$K_F$= 1.4034<br>$R^2$ = 0.7250 |

## 2.5 *Inhibitory 4–chloroaniline degradation kinetics*

Experiments were conducted in triplicate to evaluate the degradation kinetics of 4–CA. Biochar (0.5 g) and/or GRSW2–B1 ($10^7$ CFU/mL) were added to LB–4CA (50 mL) containing 4–CA at concentrations ranging from 10 to 500 mg/L, and the mixtures were incubated at room temperature with shaking at 150 rpm for 72 h. The treatments involving G1 and BC–G1 were then compared. Specific degradation rates were calculated based on the remaining concentrations of 4–CA, and the 4–CA degradation kinetics were modeled using a modified Monod model (Equation 1). In addition, the inhibitory 4–CA degradation kinetics were estimated following the Haldane, Andrews, Edwards, and Aiba models (Equations 2 to 5) [19]. The kinetic parameters were estimated by fitting models to the experimental data using non–linear regression, implemented with the Solver function in Microsoft Excel. The estimated parameters and corresponding root mean square error (RMSE) were then examined by the Solver function. The RMSE value represented the difference between the predicted and observed values as shown in Equation 6. A lower RMSE indicated a better fit of the model to the experimental data.

$$q = q_{max} \frac{S}{K'_s + S} \quad (1)$$

$$q = \frac{q_{max} S}{(S + (\frac{S^2}{K'_i}) + K'_s + (\frac{S K'_s}{K_i}))} \quad (2)$$

$$q = \frac{q_{max}}{(1 + (\frac{K'_s}{S}) + (S + K'_i))} \quad (3)$$

$$q = q_{max} \left(\exp^{-(\frac{S}{K'_i})} - \exp^{-(\frac{S}{K'_s})}\right) \quad (4)$$

$$q = \frac{q_{max} S}{(S + K'_s)} \left(\exp^{-(\frac{S}{K_i})}\right) \quad (5)$$

q and $q_{max}$ (1/h) represent the predicted and maximum specific degradation rates, respectively; S (mg/L) is the initial 4–CA concentration; $K'_s$ (mg/L) is the modified half–velocity constant; and $K'_i$ (mg/L) is the substrate inhibition constant.

$$\text{RMSE} = \sqrt{\frac{1}{n}\sum_{i=1}^{n}(P - A)^2} \quad (6)$$

P and A are the predicted and actual values, respectively; n is the number of data points.

### 2.6 *Biochar and microbial secretion characterization*

The surface functional groups of biochar (before and after use) were analyzed via FTIR spectroscopy (TENSOR27, Bruker, USA). Prior to the analysis, the biochar samples were oven–dried at 60 °C for 24 h. The surface functional groups were assessed in relation to 4–CA adsorption and enhanced biodegradation, and morphological changes of the biochar were examined via field–emission scanning electron microscopy (FE–SEM; Mira 4, TESCAN, Czech Republic). The surface areas were examined (NOVA2200E, Quantachrome, USA). The biochar samples were cleaned, fixed, dehydrated, and gold–coated following the procedure described by Sonsuphab *et. al*., [18].

Selected water samples were characterized in terms of secreted organic carbon for the systems involving G1 and BC–G1 using a fluorescence spectrofluorometer (FS5, Edinburgh Instruments, United Kingdom). The excitation wavelength was scanned from 200 to 500 nm in 5 nm increments, and emission spectra were recorded from 250 to 550 nm in 1 nm increments. It is noted that the selected wavelengths cover the typical excitation and emission wavelengths of common biological and chemical molecules [20]. The excitation and emission bandwidths were set at 5 nm, and all samples were analyzed in duplicate. An EEM analysis of deionized water was also performed daily as a blank prior to the sample measurements. An inner–filter correction was performed using UV–Vis absorption data to adjust for the attenuation of lamp light by dissolved organic carbon (DOC) molecules [20]. The cumulative volume of fluorescence intensities was examined based on regional integration.

### 2.7 *Analytical procedures*

The analytical procedure was conducted following the method described by Jenjaiwit *et. al.,* [21]. Briefly, 4–CA and its intermediate products (4–CC, AN, and CT) were analyzed via high–performance liquid chromatography (HPLC) using a C18 column and UV detector (LC2050, Shimadzu, Japan) under isocratic conditions. Prior to the analysis, the samples were filtered through a 0.2–µm nylon syringe filter and stored in an amber vial at 4 °C. A sample injection volume of 20 µL was used for HPLC, and acetonitrile and deionized water were used as the mobile phase in a ratio of 75:25 (v/v), with a flow rate of 1.0 L/min. It is noted that 4–CA and its potential intermediate products were simultaneously detected. The retention times of the peaks corresponding to 4–CA, AN, 4–CC, and CT were 4.2, 4.0, 3.7, and 3.2 min, respectively, and the detection limit of 4–CA and its intermediates was 0.1 mg/L.

For bacterial enumeration, the bacterial plate count technique was used to estimate the number of viable bacteria in a sample [18].

## 3 Results and Discussion

### 3.1 *4–chloroaniline removal*

#### *3.1.1 Adsorption of 4–CA by BC*

The 4–CA adsorption potential of the carbonized waste was first examined in an aqueous solution with an initial 4–CA concentration of 10 mg/L. 4–CA adsorption occurs rapidly and reaches equilibrium at approximately 36 h, demonstrating the preliminary effectiveness of carbonized waste for environmental abatement. The 4–CA adsorption kinetics and isotherms were then investigated, with the corresponding model equations and parameters summarized in Table 1. Considering the $R^2$ values, adsorption is better described by the pseudo–second–order model ($R^2 = 0.9970$) than the pseudo–first–order model ($R^2 = 0.9882$). Similar findings have also been reported for the adsorption of aniline–based compounds [22], [23]. Theoretically, the pseudo–first–order kinetic model indicates that the adsorption process is mainly influenced by physical interactions and surface diffusion, whereas adsorption following the pseudo–second–order kinetic model is governed by chemical interactions, such as electron exchange or surface complexation [10], [21], [23].

In this study, the pseudo–second–order model with a higher $R^2$ value implies that the sorption process is likely controlled by chemical interaction mechanisms rather than being governed solely by the 4–CA concentration. Contaminant adsorption depends on many processes, such as bulk and/or intra–particle diffusion and contaminant–biochar interactions. To evaluate the adsorption capacity, 4–CA isotherm experiments were conducted at initial 4-CA concentrations of 0.5, 1, 5, 10, 20, 40, 60, 80, and 100 mg/L over a 96–h period, with the adsorption efficiency ranging from 98.2 to 99.3%. The Langmuir model provides a better fit, indicating monolayer adsorption on a homogeneous surface, with a maximum adsorption capacity of 4.9 mg/g (Table 1). The model fitting was consistent with the previous

study [22]. Also, the changes observed in the FTIR spectra (detailed result presented in sub–section 3.3) confirmed that 4–CA adsorption is based on surface functional groups, which is likely refer to monolayer adsorption described by the Langmuir model. It was noticed that $Q_e$ (0.03 mg/g) and $Q_m$ (4.95 mg/g) values were obviously different. The difference between $Q_e$ and $Q_m$ could imply that the adsorption sites were not fully occupied under the tested equilibrium conditions. This may influence from the relatively low initial 4–CA concentration, diffusion limitation, or sorbent surface characteristics. The mechanism of this phenomenon should be further examined.

Figure 1a depicts the efficiency of 4–CA adsorption in synthetic contaminated wastewater (initial concentrations of 10–500 mg/L with other constituents, as described in Section 2). The 4–CA concentration decreases rapidly within the first 48 h, and a slight reduction can be observed thereafter. The biochar adsorbs 4–CA with efficiencies of 23.4–98.8%, and higher initial concentrations of 4–CA lead to a noticeable reduction in the removal efficiency.

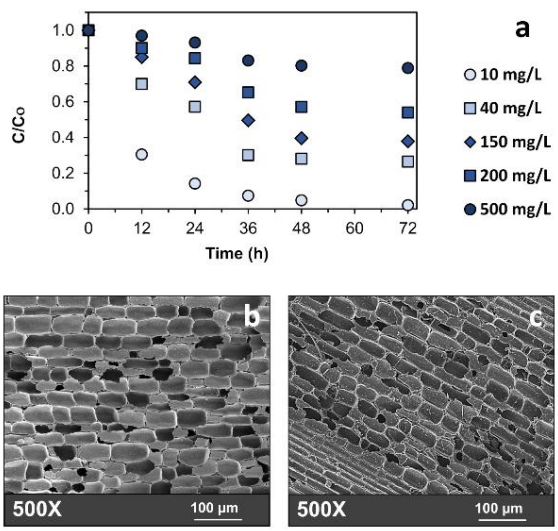


**Figure 1**: 4–CA adsorption by BC in synthetic wastewater: (a) removal efficiencies at initial 4–CA concentrations of 10 to 500 mg/L; and (b) SEM image of biochar before the experiment; and (c) SEM image of biochar after the experiment at a 4–CA concentration of 40 mg/L.

This indicates that the biochar is effective in adsorbing 4–CA in both 4–CA solution and wastewater, similar to the findings of Jenjaiwit *et. al*., [22]. However, the equilibrium time (48 h) in synthetic wastewater is longer than that in the experimental aqueous solution (36 h). The extended equilibrium period and lower 4–CA adsorption efficiencies are likely attributed to the presence of additional constituents in the LB medium, including yeast extract and tryptone, possibly competing with 4–CA for active adsorption sites on the biochar. Figures 1b and 1c are morphological characterization of biochar using FE–SEM. The carbonized waste, derived from wood vinegar production, possesses a substantial number of pores. After use, white spots observed in Figure 1c might be adsorbed 4–CA or other constituents from the 4–CA solution. Further investigation on chemical identity is required. The specific surface areas of the biochar before and after use, determined by the Brunauer–Emmett–Teller (BET) method, were 249 and 159 $m^2/g$, respectively. The lower specific surface area after use well supported the occurrence of contaminant adsorption. The 4–CA adsorption performance and material characteristics highlight the feasibility of carbonized waste as an adsorbent for organic contaminants in wastewater treatment applications.

### *3.1.2 Removal of 4–CA by G1 and BC–G1*

Figure 2 presents the 4–CA removal performances of the G1 and BC–G1 systems. The 4–CA concentration gradually decreases over a 72–h period, and different initial concentrations lead to different 4–CA removal efficiencies (Figure 2). In the G1 system, the GRSW2–B1 cells exhibit good 4–CA degradation. The degradation intermediate products were monitored along with the 4–CA quantification. 4–CA can be biodegraded through two primary pathways [11], [24]. The first pathway, which was commonly reported, 4–CA is initially converted to 4–CC, which subsequently undergoes aromatic ring cleavage to form 3–chloro–*cis,cis*–muconic acid. In the second pathway, 4–CA is dechlorinated to form AN, which is then hydroxylated to CT and further metabolized via the ortho–cleavage pathway. Among the potential intermediates (4–CC, AN, and CT), only 4–CC was detected in the early stages of the experiments, with an either reduced or undetectable concentration after 96 h. The result indicated that the 4–CA biodegradation pathway by GRSW2–B1was similar to most published works (Figure 3), where 4–CA is converted to 4–CC and 3–chloro–*cis*,*cis*-muconic acid via deoxygenation and ortho–ring cleavage, respectively [11]. The second pathway, which should detect AN and/or CT,

may not take place. Since 4–CA exhibits a higher acute toxicity compared to 4–CC and other intermediates, the degradation contributes to the detoxification of the contaminated wastewater.

As shown in Figure 2, BC–G1 shows a substantially better 4–CA removal performance than G1, with a similar trend under different concentrations. At lower 4–CA concentrations (10–100 mg/L), G1 achieves 4–CA removal efficiencies of 33–45%, while BC-G1 leads to higher removal rates of 61–73%. These results indicate that GRSW2–B1 possesses the capacity to remove 4–CA, and in the BC–G1 system, both the biodegradation and adsorption mechanisms predominantly contribute to an enhanced removal efficiency (Figure 2). In contrast, at higher initial concentrations (150–500 mg/L), the removal performance of both systems is noticeably reduced, with G1 and BC-G1 removing only 2–17% and 6–28% of 4–CA, respectively (Figure 2(a)). 4–CA served as the sole carbon source for microbial growth; therefore, the 4–CA removal efficiency increased with increasing 4–CA concentration. However, the lower removal efficiencies at high concentrations are likely due to the toxic effects of 4–CA, which inhibits microbial growth and, consequently, reduces the overall removal efficiency [24]. This finding is consistent with previous studies reporting an improved contaminant removal efficiency after biochar addition [25], [26]. Details of the inhibitory kinetics and mechanism are presented in the following section.

FE–SEM analysis of the microbial cell morphology (Figure 2(b) and (c)) reveals that the GRSW2–B1 cells in the G1 system exhibit signs of structural deterioration; this is indicated by cell deformations (Figure 2(c)), likely resulting from direct exposure to 4–CA and subsequent cellular damage. On the other hand, the GRSW2–B1 cells in the BC–G1 system appear morphologically intact. The presence of EPSs produced by the cells likely facilitates cell attachment and colonization on the biochar. At the end of the experiments (72 h) under initial 4–CA concentrations (10–80 mg/L), microbial cells of approximately $10^7$ CFU/mL were detected in the treated wastewater, while biochar–colonized cells of $10^6$–$10^7$ CFU/mL were found. At higher initial 4–CA concentrations (100–500 mg/L), lower cell numbers were detected in both the wastewater ($10^5$–$10^6$ CFU/mL) and on the biochar ($10^4$–$10^5$ CFU/mL). These results suggest that biochar can protect the microbial cells to some extent.

The findings from both the cell enumeration and morphological observations support the observed 4–CA removal efficiencies. The integration of biochar with microbial cells demonstrates various advantages, including enhanced contaminant adsorption, a reduction in the direct exposure of cells to toxic compounds, and a more favorable microenvironment for microbial growth and activity.

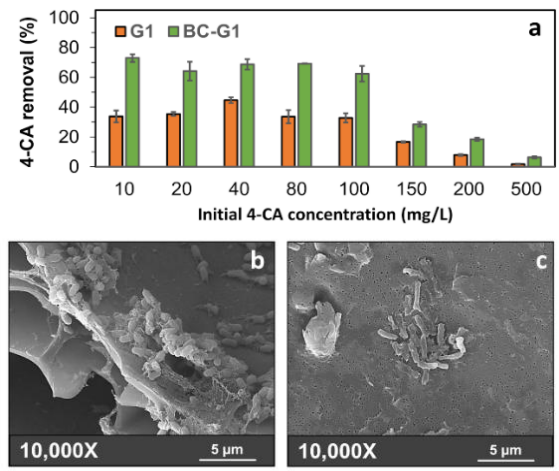


**Figure 2**: 4–CA removal by G1 and BC–G1: (a) removal efficiencies at initial 4–CA concentrations of 10 to 500 mg/L, (b) SEM image of microbial cells in BC–G1 after the experiment at a 4–CA concentration of 40 mg/L, and (c) SEM image of microbial cells in G1 after the experiment at a 4–CA concentration of 40 mg/L.

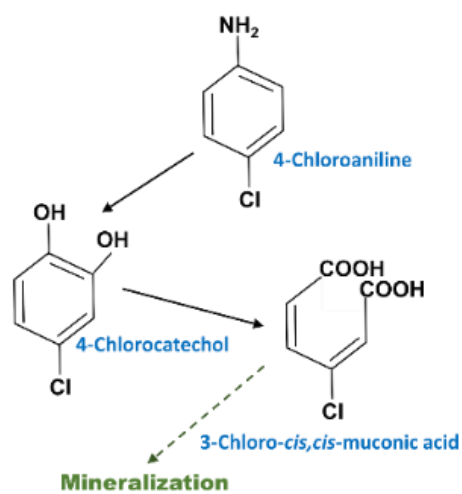


**Figure 3**: Proposed 4–CA degradation pathway.

### 3.2 *Kinetics of 4–CA degradation*

The kinetics of 4–CA degradation by G1 and BC–G1 were investigated at the initial concentrations of 1–500 mg/L using a modified Monod equation (Table 2). Due to limited microbial growth observed during the experiments, the correlation between the initial 4–CA concentration and the 4–CA removal rate was employed. As shown in Figure 4, 4–CA degradation is inhibited at high initial concentrations; inhibitory kinetic models were thus applied to describe the degradation behavior (Table 2).

Considering the RMSE values shown in Table 2, the Andrews model provides the best fit for both the G1 and BC–G1 systems. It is observed that the Edwards model provided a similar RMSE value only for the G1 system. In addition, the 4–CA removal rates substantially decrease at high concentrations due to toxicity. The maximum threshold concentration at which the microorganism can effectively degrade toxic contaminants varies. According to the model estimations, 4–CA begins self-substrate inhibition at a concentration of 65 mg/L in both systems. In general, the Andrews model describes the main inhibitory effect of high substrate concentrations on microbial growth and substrate degradation [27]. Compared to the study by Taweetanawanit *et. al.,* [28] on the degradation of another chlorinated aniline, triclocarban biodegradation kinetics were better described by the Edwards model, which assumes that substrate degradation is inhibited by both the toxic substrate and its toxic degradation intermediates. Triclocarban is much more toxic compared to 4–CA and produces toxic degradation intermediates, including 4–CA. In this study, 4–CC, a detected intermediate, is less toxic and may not affect the degradation kinetics. As a result, a different kinetic model appropriately described the degradation behavior observed in this study. The Andrews model was fitted to the data in this study because 4–CA itself constitutes the toxic substance; therefore, high concentrations of 4–CA inhibit microbial growth and 4–CA removal.

Notably, other kinetic constants ($q'_{max}$ and $K'_S$) from BC–G1 are higher than those from G1. This could be attributed to the partial immobilization of microbial cells on the biochar (Figure 2b), which likely reduces their direct exposure to 4–CA, maintains cell viability, and supports 4–CA degradation. Additionally, the biochar may contribute to 4–CA removal via adsorption or enhanced biodegradation processes, potentially by promoting electron transfer processes.

**Table 2**: 4–CA degradation kinetic parameters following the modified Monod and inhibitory degradation models.

| Model | Parameters | | | RMSE |
|---|---|---|---|---|
| | $q_{max}$ (mg/h-CFU) | $K'_s$ (mg/L) | $K'_i$ (mg/L) | |
| **G1** | | | | |
| Modified-Monod | $0.47\times10^{-4}$ | 93.79 | - | - |
| Haldane | $2.14\times10^{-4}$ | 150.37 | 50.37 | $5.18\times10^{-6}$ |
| Andrews | $1.18\times10^{-4}$ | 126.19 | 64.23 | $3.55\times10^{-6}$ |
| Edwards | $9.76\times10^{-4}$ | 159.62 | 175.08 | $4.26\times10^{-6}$ |
| Aiba | $5.03\times10^{-4}$ | 227.26 | 33.75 | $18.2\times10^{-6}$ |
| **BC-G1** | | | | |
| Modified-Monod | $0.87\times10^{-4}$ | 173.88 | - | - |
| Haldane | $6.96\times10^{-4}$ | 341.11 | 46.21 | $8.61\times10^{-6}$ |
| Andrews | $2.70\times10^{-4}$ | 245.84 | 65.50 | $6.28\times10^{-6}$ |
| Edwards | 2.50 | 128.31 | 128.27 | $142.20\times10^{-6}$ |
| Aiba | $6.35\times10^{-4}$ | 189.62 | 49.54 | $27.58\times10^{-6}$ |

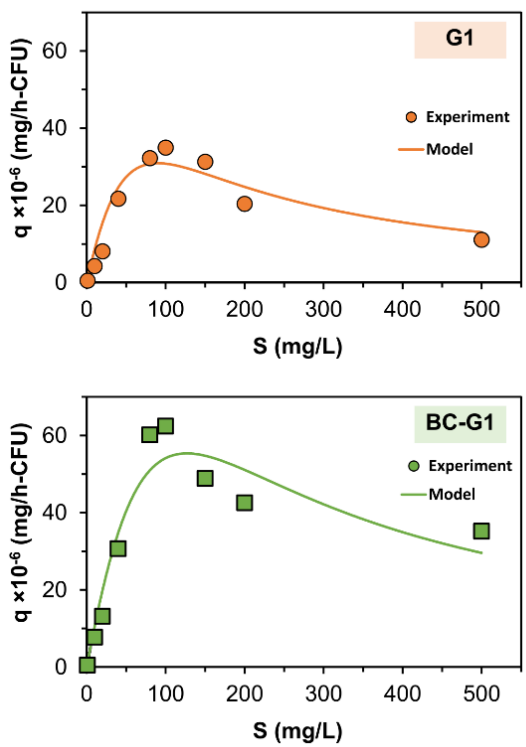


**Figure 4**: Inhibitory 4–chloroaniline degradation kinetics of G1 and BC–G1 systems, following the Andrews model.

### 3.3 *Role of biochar in 4–CA removal*

Based on the guidelines from the International Biochar Initiative, the elemental properties of biochar with common threshold values of $H/C_{org} \leq 0.7$ and $O/C_{org} \leq 0.6$ were defined [29]. In our previous work, we quantified the elemental composition of biochar derived from wood-vinegar production waste [30]. The calculated molar ratios of $H/C_{org}$ and $O/C_{org}$ were 0.16 and 0.05, respectively, which are in the acceptable range to classify the material as biochar. Biochar plays several possible roles in contaminant removal. Biochar contains abundant surface functional groups and porous structures that can facilitate contaminant adsorption on its surface or EPS–coated surface. The FTIR and FE–SEM analyses well characterize these phenomena. Additionally, biochar can enhance biodegradation by promoting electron transfer processes within the microbial cells. These properties can be inferred from FTIR and EEM characterization. In this study, the heated carbonized waste exhibited main FTIR peaks associated with carbon and oxygen–containing functional groups (Figure 5a), consistent with characteristics of common biochar reported in previous studies [10], [23]. Also, from our previous work on elemental analysis of the carbonized waste revealed that carbon (89.22%) and oxygen (6.20%) were the dominant elements [30]. These results suggest that the heated carbonized waste was effectively converted into biochar.

4–CA exhibits good adsorption on biochar, as described earlier. Figure 5 depicts the surface chemical functional groups of biochar, as identified via FTIR spectroscopy. As shown in Figure 5a, distinct changes in the functional groups on the biochar surface before and after adsorption can be observed at four specific wave numbers: 866, 1060, 1350–1700, and 1880 $cm^{-1}$. These correspond to C=C bending, C–O stretching, C=O and C=C stretching, and C=O stretching vibrations, respectively, consistent with a previous study on the adsorption of chlorinated aniline compounds [22]. Typically, 4–CA contains a benzene ring with an amine group and a chlorine atom; therefore, the corresponding FTIR peaks are C–H stretching, N–H stretching and C–Cl stretching vibration, respectively. According to the results reported by Anitha *et. al.,* [31], the peaks at 1493 and 1614 $cm^{-1}$ indicate C–C stretching vibrations in the benzene ring, while the peaks at 823 and 1283 $cm^{-1}$ confirm C–Cl and C–N stretching vibrations, respectively. Their findings showed that these characteristic peaks were related to the changes observed for biochar in this study. This states that the FTIR characterization from the previous work and this study supports the occurrence of 4–CA adsorption on the biochar surface.

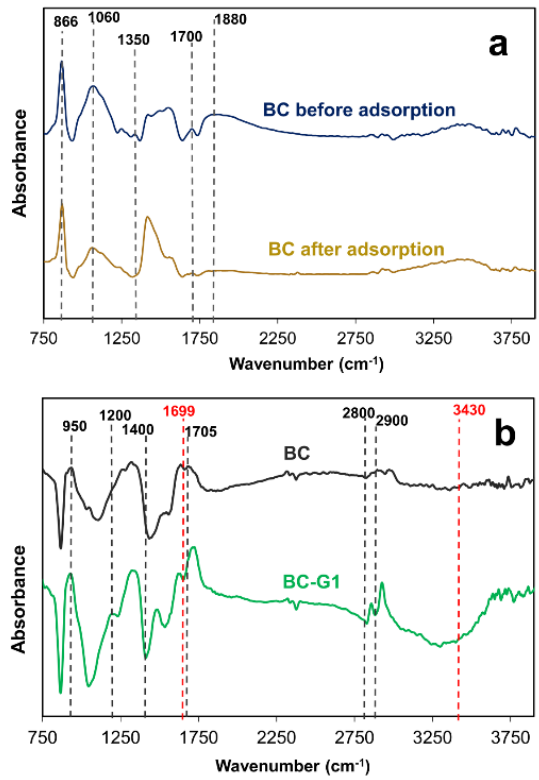


**Figure 5**: FTIR spectra of biochar (a) before and after adsorption with a 4–CA solution (40 mg/L), and (b) after 4–CA contaminated wastewater treatment (40 mg/L). In (a), "BC before adsorption" is pristine biochar, and "BC after adsorption" is biochar recovered after the adsorption test. In (b), "BC" is biochar recovered after the wastewater treatment by only biochar, and "BC–G1" is biochar recovered from the treatment by combined biochar and GRSW2–B1.

Considering the 4–CA removal results presented in Figures 1 and 2, 4–CA adsorption reaches equilibrium at 48 h. However, BC–G1 leads to a consistent decrease in the 4–CA concentrations (e.g., for the experiments at the initial 4–CA concentrations of 40 and 80 mg/L). From 48 to 72 h, the G1 system exhibits a lower degree of 4–CA degradation than BC–G1. These findings suggest that biochar not only contributes to 4–CA adsorption but also enhances biodegradation, accelerating the overall 4–CA removal process. Figure 5(b) shows the surface

functional groups of the biochar for the BC–G1 and BC systems after 4–CA removal. According to the FTIR observation, BC–G1 exhibits increased peaks corresponding to EPSs, including polysaccharides (950–1200 $cm^{-1}$), proteins (1400–1705 $cm^{-1}$), and lipids (2800–2900 $cm^{-1}$) [10], [18], [23]. The FTIR and FE–SEM results confirm that the microbial cells in BC–G1 can grow and secrete EPSs to form biofilms, which likely minimize direct exposure to toxic compounds, extending cell viability and improving the 4–CA removal efficiency. In addition, the presence of EPSs on the biochar surface can further promote 4–CA adsorption. This is consistent with a previous work reporting the efficient adsorption of organic contaminants by EPSs [32].

The FTIR spectrum of BC–G1 (Figure 5(b)) displays functional group changes at 1699 and 3430 $cm^{-1}$, which correspond to C=O and –OH groups related to quinones/phenazines and hydroquinones, respectively. These oxygen–containing functional groups display redox-active properties [6] and facilitate DIET, leading to the promotion of contaminant biodegradation [15], [25], [33].

Figure 6 shows the EEM spectra of untreated, G1–treated, and BC–G1–treated wastewater at initial 4–CA concentrations of 20 and 150 mg/L. The spectra are divided into five regions—Regions I, II, III, IV, and V—representing aromatic protein I, aromatic protein II, fulvic acid–like, soluble microbial product–like, and humic acid–like compounds, respectively [20]. In Figure 6, the fluorescence intensities from the samples treated with 40 mg/L and 150 mg/L 4–CA appear to be only slightly different. This is likely because the background from the synthetic wastewater was substantially higher than the DOC contributed by 4–CA. Therefore, cumulative volumes of fluorescence intensities in each region were examined to identify the differences of DOC composition related to substrate concentration and potential toxicity. Overall, 4–CA–contaminated wastewater at different concentrations shows slight differences in the fluorescence intensities for all regions (Figure 7). Comparing the untreated and treated wastewater, the latter exhibits increased fluorescence intensities (Figure 7). Notably, Region II, associated with simple aromatic proteins II—commonly reported as exoenzymes and potential electron shuttles in microbial electron transfer processes—shows noticeable increases. Region III, fulvic acid-like compounds—known as electron mediators—also exhibit higher intensities [34], [35], as is the case for Region IV (soluble microbial by–product–like compounds). These soluble EPS components have been reported to contribute to biosorption [36]. Region V represents redox–active humic acid–like compounds, which are quinone functional groups and capable of mediating electron transfer [37].

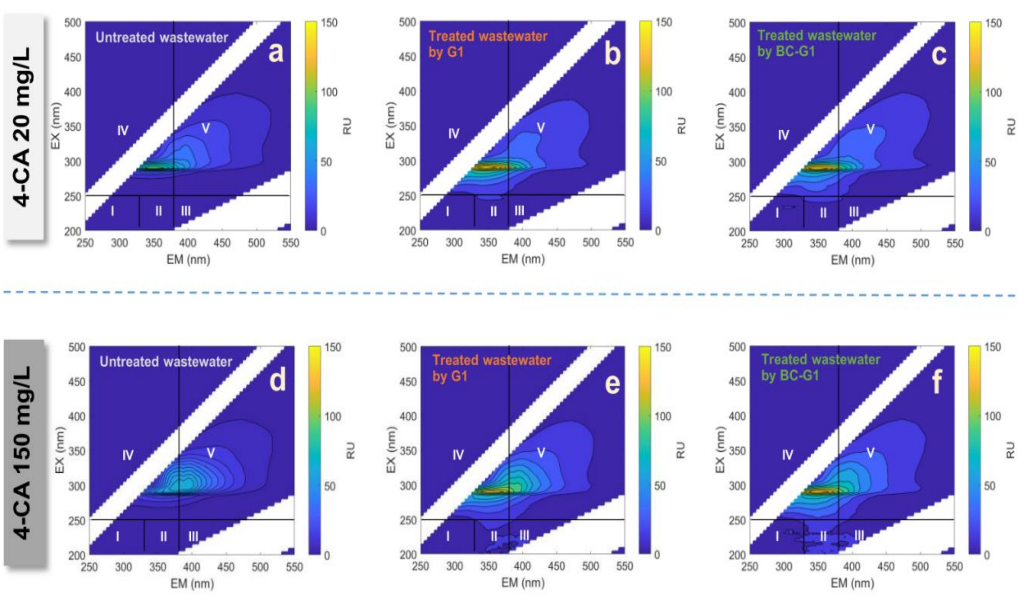


**Figure 6**: EEM spectra of (a) and (d) synthetic contaminated wastewater, (b) and (e) G1–treated wastewater, and (c) and (f) BC–G1–treated wastewater at 4–CA concentrations of 20 and 150 mg/L, respectively.

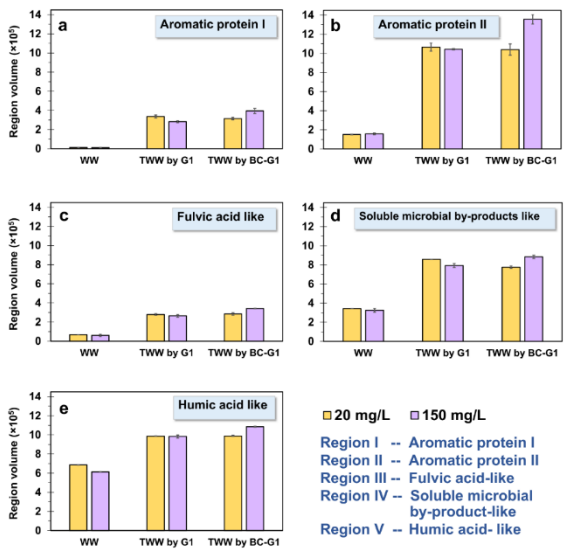


**Figure 7**: Fluorescence intensities of synthetic contaminated wastewater (WW) and treated wastewater (TWW) at 4–CA concentrations of 20 and 150 mg/L: (a) aromatic protein I, (b) aromatic protein II, (c) fulvic acid–like, (d) soluble microbial by–product–like, and (e) humic acid–like compounds.

Comparing the G1– and BC–G1–treated wastewater at a 4–CA concentration of 20 mg/L, no significant differences in the fluorescence intensities were observed across all regions. This suggests that at low 4–CA concentrations, microbial degradation is sufficient, and biochar has a negligible positive effect on DIET. In contrast, at 150 mg/L 4–CA, the fluorescence intensity in Region II of BC–G1 is significantly higher than that of G1 (Figure 7b). These findings indicate that biochar facilitates increased electron shuttling in DIET, potentially due to aromatic protein II production [34], [35]. Furthermore, the higher intensity in Region V of BC–G1 (Figure 7(e)) suggests an enhanced mediation of electron transfer induced by biochar, related to changes in the quinone functional groups, as detected by FTIR spectroscopy [37]. Region IV also shows an increase in BC–G1, suggesting that biochar can promote the production of soluble EPSs (Figure 7(d)).

This is consistent with the FTIR results and the findings of Pan *et. al.,* [38], which demonstrated that soluble EPSs, typically containing more proteins, possess a greater ability for organic contaminant adsorption. The FTIR and EEM analyses provide preliminary evidence supporting the enhanced electron transfer processes. However, to clearly elucidate the mechanisms, electrochemical analyses should be performed in future work.

The enhanced 4–CA removal observed in the BC–G1 system can be attributed to the multifunctional roles of biochar, which contribute through two primary mechanisms: adsorption and enhanced biodegradation [25]. In the first mechanism, 4–CA is initially adsorbed onto the biochar surface, with the biochar also stimulating EPS production, increasing the overall sorption capacity. In the second mechanism, biochar reduces the direct exposure of microbial cells to toxic contaminants, improving cell viability, with the biochar promoting electron transfer processes. These two processes facilitate greater microbial degradation. Overall, the findings highlight the potential of carbonized wood waste-derived biochar for the sustainable and efficient remediation of emerging toxic contaminants.

## 4 Conclusions

This study presents the effective removal of 4-CA through the integration of carbonized wood waste-derived biochar and microbial cells. The biochar, containing numerous pores and various functional surfaces, provided good 4-CA adsorption (following the Langmuir model), with a maximum adsorption capacity of 4.9 mg/g. The combination of biochar and GRSW2-B1 exhibited 4-CA removal efficiencies of up to 73%, while using GRSW2-B1 cells alone resulted in up to 45% 4-CA degradation. However, 4-CA removal was inhibited at high concentrations. The 4-CA degradation kinetics of both the G1 and BC-G1 systems followed the Andrews model, with an inhibition concentration of 65 mg/L.

The synergistic removal of 4-CA identified in the BC-G1 system is attributed to the roles of biochar, including enhanced adsorption and biodegradation. This is the first study to confirm these roles with regard to 4-CA removal via FE-SEM, FTIR, and EEM analyses. Biochar not only enabled direct adsorption on its surface but also stimulated EPS production, which likely contributes to 4-CA adsorption. Moreover, as a porous material, biochar reduced the direct exposure of microbial cells to high 4-CA concentrations, which ensured their survival and degradation activity. The spectroscopic evidence suggests that biochar may facilitate electron transfer processes, thereby promoting enhanced 4-CA biodegradation.

In the future, long-term operation in a continuous-flow wastewater treatment system, along

with electrochemical analyses to evaluate the electron transfer mechanisms, should be conducted to further verify the findings of this study. Overall, our findings underscore the potential of the integrated biochar-and-microbial system for the sustainable and effective remediation of emerging toxic contaminants. The use of carbonized wood waste as biochar also supports resource recovery within the framework of Sustainable Development Goal 6.

## Acknowledgments

This work was supported by the Faculty of Engineering, Khon Kaen University, which received funding from the Fundamental Fund 2026-2027 (National Science, Research, and Innovation Fund [NSRF], Thailand) and the Research Administration Division, Khon Kaen University, Thailand. Grants were also received from the Research Center for Environmental and Hazardous Substance Management (Khon Kaen University, Thailand). The authors would like to thank the Department of Environmental Engineering (Faculty of Engineering, Khon Kaen University, Thailand) for equipment support.

## Author Contributions

T.B.: methodology, validation, formal analysis, investigation, writing an original draft; S.J.: methodology, formal analysis, investigation, reviewing and editing; P.J.: methodology, formal analysis, investigation, reviewing and editing; T.R.: methodology, formal analysis, investigation, reviewing and editing; S.S.-R.: conceptualization, data curation, writing—reviewing and editing, funding acquisition, project administration. All authors have read and agreed to the published version of the manuscript.

## Conflicts of Interest

The authors declare no conflict of interest.

## Declaration of generative AI and AI-assisted technologies in the writing process

The authors utilized the ChatGPT tool to enhance the language and readability of the manuscript.

## References

[1] S. Jenjaiwit, S. Siripattanakul-Ratpukdi, T. Ratpukdi, and A. Youngwilai, "Performance and pathway of 4-chloroaniline degradation: A comparative study of electro-peroxone, ozonation, and electrolysis processes," *Applied Science and Engineering Progress*, vol. 19, no. 7777, 2026, doi: 10.14416/j.asep.2025.05.009.

[2] D. Zhang et al., "Risk assessments of emerging contaminants in various waters and changes of microbial diversity in sediments from Yangtze River chemical contiguous zone, Eastern China," *Science of the Total Environment*, vol. 803, 2022, Art. no. 149982, doi: 10.1016/j.scitotenv.2021.149982.

[3] L. L. Zhang et al., "Biodegradation of 2-chloroaniline, 3-chloroaniline, and 4-chloroaniline by a novel strain *Delftia tsuruhatensis* H1," *Journal of Hazardous Materials*, vol. 179, pp. 875–882, 2010, doi: 10.1016/j.jhazmat.2010.03.086.

[4] M. A. M. Salleh et al., "Cationic and anionic dye adsorption by agricultural solid wastes: A comprehensive review," *Desalination*, vol. 280, pp. 1–13, 2011, doi: 10.1016/j.desal.2011.07.019.

[5] Y. Gao et al., "Intrinsic properties of biochar for electron transfer," *Chemical Engineering Journal*, vol. 475, 2023, Art. no. 146356, doi: 10.1016/j.cej.2023.146356.

[6] S. Ren et al., "Hydrochar-facilitated anaerobic digestion: evidence for direct interspecies electron transfer mediated through surface oxygen-containing functional groups," *Environmental Science & Technology*, vol. 54, pp. 5755–5766, 2020, doi: 10.1021/acs.est.0c00112.

[7] D. R. Lima et al., "Comparison of acidic leaching using a conventional and ultrasound-assisted method for preparation of magnetic-activated biochar," *Journal of Environmental Chemical Engineering*, vol. 9, 2021, Art. no. 105865, doi: 10.1016/j.jece.2021.105865.

[8] J. Yan et al., "Mechanism insight into sulfidated nano zero-valent iron/biochar activated persulfate for highly efficient degradation of p-chloroaniline," *Chemosphere*, vol. 375, 2025, Art. no. 144229, doi: 10.1016/j.chemosphere.2025.144229.

[9] S. Sangsuk, S. Suebsiri, and P. Puakhom, "The metal kiln with heat distribution pipes for high

quality charcoal and wood vinegar production," *Energy for Sustainable Development*, vol. 47, pp. 149–157, 2018, doi: 10.1016/j.esd.2018.10.002.

[10] A.B.D. Nandiyanto, A.E. Putri, M. Fiandini, R. Ragadhita, and T. Kurniawan, "Biochar microparticles from pomegranate peel waste: literature review and experiments in isotherm adsorption of ammonia," *Applied Science and Engineering Progress*, vol. 18, no. 1, 2025, Art. no. 7506, doi: 10.14416/j.asep.2024.08.009.

[11] P. Hongsawat and A. S. Vangnai, "Biodegradation pathways of chloroanilines by *Acinetobacter baylyi* strain GFJ2," *Journal of Hazardous Materials*, vol. 186, pp. 1300–1307, 2011, doi: 10.1016/j.jhazmat.2010.12.002.

[12] M. Zhu et al., "Biodegradation characteristics of p-chloroaniline and the mechanism of co-metabolism with aniline by *Pseudomonas* sp. CA-1," *Bioresource Technology*, vol. 406, 2024, Art. no. 131086, doi: 10.1016/j.biortech.2024.131086.

[13] N. Kataoka, T. Tajima, J. Kato, W. Rachadech, and A. S. Vangnai, "Development of butanol-tolerant *Bacillus subtilis* strain GRSW2-B1 as a potential bioproduction host," *AMB Express*, vol. 1, no. 10, p. 10, 2011, doi: 10.1186/2191-0855-1-10.

[14] K. Wang et al., "The dual role of biochar in boosting phenol biodegradation and anti-inhibition performance against hazardous substrate," *Journal of Environmental Chemical Engineering*, vol. 12, 2024, Art. no. 113747, doi: 10.1016/j.jece.2024.113747.

[15] Q. Wang et al., "Cr(VI) bioreduction enhanced by the electron transfer between flavin reductase and persistent free radicals," *Chemosphere*, vol. 368, 2024, Art. no. 143746, doi: 10.1016/j.chemosphere.2024.143746.

[16] S. Niu et al., "Biochar, microbes, and biochar-microbe synergistic treatment of chlorinated hydrocarbons in groundwater: A review," *Frontiers in Microbiology*, vol. 15, 2024, Art. no. 1443682, doi: 10.3389/fmicb.2024.1443682.

[17] Y. Li et al., "Biochar-induced quorum sensing enhances methane production by strengthening direct interspecies electron transfer," *Bioresource Technology*, vol. 434, Art. no. 132845, 2025, doi: 10.1016/j.biortech.2025.132845.

[18] K. Sonsuphab, et al., "Integrated remediation and detoxification of triclocarban-contaminated water using waste-derived biochar-immobilized cells by long-term column experiments," *Environmental Pollution*, vol. 357, 2024, Art. no. 124456, doi: 10.1016/j.envpol.2024.124456.

[19] N. Therdkiattikul, T. Ratpukdi, P. Kidkhunthod, N. Chanlek, and S. Siripattanakul-Ratpukdi, "Manganese-contaminated groundwater treatment by novel bacterial isolates: Kinetic study and mechanism analysis using synchrotron-based techniques," *Scientific Reports*, vol. 10, 2020, Art. no. 13391, doi: 10.1038/s41598-020-70355-w.

[20] N. Ranthom, W. Khongnakorn, and P. Jutaporn, "MIEX resin and enhanced coagulation treatment of high-bromide natural water: Chlorine reactivity and DBP precursors removal," *Journal of Environmental Chemical Engineering*, vol. 11, 2023, Art. no. 111497, doi: 10.1016/j.jece.2023.111497.

[21] S. Jenjaiwit et al., "Electro-peroxone process for triclocarban and triclosan removal and reclaimed water disinfection," *Journal of Water Process Engineering*, vol. 67, 2024, Art. no. 106200, doi: 10.1016/j.jwpe.2024.106200.

[22] S. Jenjaiwit et al., "Removal of triclocarban from treated wastewater using cell-immobilized biochar as a sustainable water treatment technology," *Journal of Cleaner Production*, vol. 320, 2021, Art. no. 128919, doi: 10.1016/j.jclepro.2021.128919.

[23] A. G. Bermúdez, M. J. A. Arias, J. C. Mosquera, and D. J. M. Castro, "Ferromagnetic biochar derived from agricultural waste of *Musa acuminata* for adsorption of dyes," *Applied Science and Engineering Progress*, vol. 18, no. 4, 2025, Art. no. 7792, doi: 10.14416/j.asep.2025.06.004.

[24] Y. Bo et al., "Elucidating the co-metabolism mechanism of 4-chlorophenol and 4-chloroaniline degradation by *Rhodococcus* through genomics and transcriptomics," *Environmental Research*, vol. 274, 2025, Art. no. 121362, doi: 10.1016/j.envres.2025.121362.

[25] S. Wang et al., "Mechanistic insight into enhancement of undissolved rice husk biochar on tetracycline biodegradation by strain *Serratia marcescens* based on electron transfer response," *Journal of Hazardous Materials*, vol. 491, 2025, Art. no. 137895, doi: 10.1016/j.jhazmat.2025.137895.

[26] C. Xia et al., "Chromium(VI) and nitrate removal from groundwater using biochar-assisted zero valent iron autotrophic bioreduction: Enhancing electron transfer efficiency and reducing EPS

accumulation," *Environmental Pollution*, vol. 364, 2025, Art. no. 125313, doi: 10.1016/j.envpol.2024.125313.

[27] J. F. Andrews, "A mathematical model for the continuous culture of microorganisms utilizing inhibitory substrates," *Biotechnology and Bioengineering*, vol. 10, pp. 707–723, 1968, doi: 10.1002/bit.260100602.

[28] P. Taweetanawanit, T. Ratpukdi, and S. Siripattanakul-Ratpukdi, "Performance and kinetics of triclocarban removal by entrapped *Pseudomonas fluorescens* strain MC46," *Bioresource Technology*, vol. 274, pp. 113–119, 2019, doi: 10.1016/j.biortech.2018.11.085.

[29] International Biochar Initiative. "Standardized product definition and product testing guidelines for biochar that is used in soil (IBI Biochar Standards, Version 2.1)." biochar-international.org. Accessed: Nov. 11, 2015. [Online.] Available: https://biochar-international.org/wp-content/uploads/2020/06/IBI_Biochar_Standards_V2.1_Final2.pdf

[30] A. Youngwilai et al., "Characterization of dissolved organic carbon and disinfection by-products in biochar filter leachate using orbitrap mass spectrometry," *Journal of Hazardous Materials*, vol. 424, 2022, Art. no. 127691, doi: 10.1016/j.jhazmat.2021.127691

[31] T.R. Anitha et al., "Growth and characterization of organic 4-chloroaniline single crystals for nonlinear optical applications," *Journal of Materials Science: Materials in Electronics*, vol. 35, Art. no. 1324, 2024, doi: 10.1007/s10854-024-13063-9.

[32] L. Huang et al., "A review of the role of extracellular polymeric substances (EPS) in wastewater treatment systems," *International Journal of Environmental Research and Public Health*, vol. 19, 2022, Art. no. 12191, doi: 10.3390/ijerph191912191.

[33] M. Wang, Z. Zhao, and Y. Zhang, "Magnetite-contained biochar derived from Fenton sludge modulated electron transfer of microorganisms in anaerobic digestion," *Journal of Hazardous Materials*, vol. 403, 2021, Art. no. 123972, doi: 10.1016/j.jhazmat.2020.123972.

[34] Y. Wang et al., "Insights into the influence of $Fe_2NiO_4$ nanoparticles on biomethanation of $H_2$ and $CO_2$ to $CH_4$: from the standpoint of electron transfer capacity, microbial communities and metabolism," *Renewable Energy*, vol. 237, Art. no. 121709, 2024, doi: 10.1016/j.renene.2024.121709.

[35] Y. Zhu et al., "Dual roles of zero-valent iron in dry anaerobic digestion: Enhancing interspecies hydrogen transfer and direct interspecies electron transfer," *Waste Management*, vol. 118, pp. 481–490, 2020, doi: 10.1016/j.wasman.2020.09.005.

[36] J. Cheng et al., "Improving $CH_4$ production and energy conversion from $CO_2$ and $H_2$ feedstock gases with mixed methanogenic community over Fe nanoparticles," *Bioresource Technology*, vol. 314, 2020, Art. no. 123799, doi: 10.1016/j.biortech.2020.123799.

[37] D. Li et al., "Revealing synergistic mechanisms of biochar-assisted microbial electrolysis cells in enhancing the anaerobic digestion performance of waste activated sludge: Extracellular polymeric substances characterization, enzyme activity assay, and multi-omics analysis," *Water Research*, vol. 267, 2024, Art. no. 122501, doi: 10.1016/j.watres.2024.122501.

[38] X. L. Pan et al., "Binding of dicamba to soluble and bound extracellular polymeric substances (EPS) from aerobic activated sludge: A fluorescence quenching study," *Journal of Colloid and Interface Science*, vol. 345, pp. 442–447, 2010, doi: 10.1016/j.jcis.2010.02.011.